Journal of Science and Technology in Civil Engineering, HUCE, 2026, 20 (4): 111–128

MODEL ORDER REDUCTION IN STATE SPACE BASED ON OPTIMIZATION FOR SENSOR PLACEMENTS OF FRAME STRUCTURES CONSIDERING DAMPING

Tam T. N. Do[a,b], Quan M. Lieu[a,b], Qui X. Lieu[a,b,*]

[a] *Faculty of Civil Engineering, Ho Chi Minh City University of Technology (HCMUT), 268 Ly Thuong Kiet street, Dien Hong ward, Ho Chi Minh City, Vietnam*
[b] *Vietnam National University Ho Chi Minh City (VNU-HCM), Linh Xuan ward, Ho Chi Minh City, Vietnam*

Article history:
Received 06/3/2025, Revised 13/4/2025, Accepted 23/4/2026, Available online 16/10/2026, Version of Record 25/12/2026

Abstract

In Structural Health Monitoring (SHM), determining the best locations for putting measurement sensors to record the effective modal data is extremely important to serve the damage detection process. However, this implementation is often based on engineers' experience without using a specific strategy constructed on mathematical bases. Therefore, this work aims to propose an effective technique for optimization of sensor locations for frames considering damping based on a model order reduction (MOR) in state space. By maximizing all the coefficients on the main diagonal line of the modal assurance criterion (MAC) matrix, sensor positions can be optimized by the particle swarm optimization (PSO) with several modifications compared to its original form to meet the current optimization requirement. In which, design variables are integer numbers assigned to the labels of degrees of freedom (DOFs) of a structural system. Two steel frame structures containing one for 2D one-storey frame and one for 2D four-storey frame are illustrated with different sensor quantities to demonstrate the ability of the present approach. Acquired results show the potential applications to the SHM area.

Keywords: model order reduction; state space; optimal sensor placements; damped vibration; frames; modal assurance criterion.

1. Introduction

In recent decades, the SHM area has become a crucial tool for assessing the working condition, detecting early damage, as well as ensuring the operational safety of engineering structures. In which, sensors are often utilized to measure the data for identifying dynamic characteristics of a monitored structure such as natural frequencies, vibration modes, and damping coefficients, etc. Based upon those recorded signals, the structural state with different flawed levels can be estimated, aiming to release proper solutions to maintenance works [1–3].

However, in practice, the number of sensors that can be installed on a structure is often limited by equipment costs, construction conditions, and long-term maintenance requirements. Furthermore, no all measurement locations can also provide the same level of dynamic information for damage detection. Indeed, many locations may yield very small vibration signals, or contain unnecessarily redundant information, or even cause high-noise levels that can lead to unreliable accuracy, even incorrect results for modal identification and damage diagnosis. Therefore, the optimal placement of sensors plays a crucial role in improving the efficiency of SHM systems [4]. Sensor placement

*Corresponding author. *E-mail address:* lieuxuanqui@hcmut.edu.vn (Lieu, Q. X.)
https://doi.org/10.31814/stce.huce2026-20(4)-08 p-ISSN 1859-2996; e-ISSN 2734-9268
© 2026 The Author(s). Published by Hanoi University of Civil Engineering. Licensed under CC BY-NC-ND 4.0.

optimization aims to maximize an amount of useful information obtained from measurement data while still minimizing the number of sensors required. Optimal sensor placement improves the linear independence of measured vibration modes, reduces modal correlation, and increases the stability of inverse problems in structural analysis. In this context, the sensor placement optimization problem is often modeled as an optimization problem of finding the best DOFs, aiming to satisfy a given objective function and constraints. In which, the common criteria are often used to evaluate the quality of the sensor configuration that can be listed as effective independence (EFI) [5], MAC [6], or Fisher information function [7], etc. Although a variety of articles have been published, developing effective optimization methods for such a problem is still essential to improve the accuracy, reliability and scalability of modern SHM systems in the future.

Generally, the best locations for installing sensors for a structure are often searched via the optimization strategy. In order to handle this issue, meta-heuristic optimization algorithms, which are known as non-gradient-based ones, have been a prior selection. In this regard, the most commonly used algorithms can be listed such as genetic algorithms (GA) [8], monkey algorithm (MA) [9], simulated annealing (SA) [10], hierarchic wolf algorithm (HWA) [11], Jaya algorithm (JA) [12], circle-inspired optimization algorithm (CIOA) [13] and so on. The success of these algorithms is mainly thanks to the possibilities of: (i) reliably handling discrete design variables with regard to sensor locations; (ii) efficiently avoiding falling into local solutions owing to the global exploration ability; (iii) easily integrating complex objective functions based on modal criteria such as EFI, MAC, Fisher information functions, and (iv) easily extending well to large-scale structures. Due to the above-indicated advantages, many publications on applying the meta-heuristic algorithms to specifying sensor placement configurations have been studied by numerous scholars in practical engineering problems.

It can be recognized that most previous studies on sensor position optimization in the SHM are primarily devoted to the undamped free vibration structures. In these models, the optimization criteria are often established based on the vibration modes and eigenvalues acquired from the eigenvalue problems, where the influence of damping is negligible, and thus it can be ignored. It is obvious that neglecting the damping influence on sensor position optimization problems can lead to inefficient sensor configurations in practical applications, especially for parameter identification, fault detection based on dynamic responses, and systems with significant damping intensities. As a consequence, developing sensor position optimization methods that consider the effects of damping is necessary to improve the realism, accuracy, and applicability of SHM systems in engineering practice.

Along with the limitations related to the no-dampness assumption, another notable research gap lies in the application of sensor placement optimization methods to frame structures, particularly in the field of high-rise buildings. Most existing researches often focus on simple structural systems such as beams, plates, or mass-spring models, while high-rise frame structures have more complex dynamic characteristics. Indeed, in high-rise buildings, dynamic responses are heavily influenced by environmental loads such as wind and earthquakes, where damping plays a crucial role in controlling the amplitude of oscillation and energy dissipation. Therefore, recording dynamic data with damping is crucial to accurately assessing structural behavior, identifying dynamic parameters, and detecting early failures. However, current researches on sensor placement optimization for frame structures are relatively limited, particularly regarding methods that simultaneously consider the damping effects and the discrete nature of sensor placements. Ignoring these factors can lead to sensor configurations that do not fully reflect the actual dynamic responses. This can reduce the effectiveness of SHM systems in practical applications.

As indicated in Refs. [14–16], ROM techniques and sensor placement optimization are closely related because both rely on exploiting and preserving the dominant dynamic subspace of the structure. While MOR seeks to approximate the responses of a higher-order system using a small set of dominant modes or states, sensor placement optimization aims to ensure that the measured quantities provide sufficient information to accurately observe and reproduce that reduced-order subspace. Inadequate sensor placement can lead to a loss of observability which degrades the accuracy and reliability of ROMs. Therefore, selecting optimal sensor placement is crucial to ensure the effectiveness of ROMs in dynamic analysis and SHM.

From the above-discussed literature review, it can be seen that developing sensor placement optimization methods that consider the effects of damping, specifically for frame structures, is relatively limited, especially in collecting the most effective vibration data for SHM of frame structures. Consequently, this work is carried out herein.

2. Basic theories

2.1. Beam-column modeling

In this work, all beam and column members of a frame structure are simulated by the Euler-Bernoulli beam theory [17] for finite element analysis. Accordingly, the displacements at a point along the beam thickness are represented as follows

$$\begin{aligned} u(x,z) &= u_0(x) - z\theta(x) \\ w(x,z) &= w_0(x) \end{aligned} \tag{1}$$

where $z \in [-h/2, +h/2]$; u_0 and w_0 are the axial and transverse displacements defined at $z = 0$, respectively; $\theta(x) = \dfrac{\mathrm{d}w_0(x)}{\mathrm{d}x}$ is the bending rotation in the x–z plane.

Based on this theory, the axial displacement is approximated by

$$u_0(x) = \{u_1 \quad u_2\}\{N_1 \quad N_2\}^{\mathrm{T}} \tag{2}$$

where u_1 and u_2 denote the axial displacement at nodes 1 and 2 of the beam element, respectively. N_1 and N_2 stand for the first-order Lagrange functions.

Meanwhile, the transverse displacement is approximated by four third-order Hermite polynomials, i.e. $N_i^w(x)$ $(i = 1 \rightarrow 4)$, by

$$w_0(x) = \{N_1^w \quad N_2^w \quad N_3^w \quad N_4^w\} \begin{Bmatrix} w_1 \\ \theta_1 \\ w_2 \\ \theta_2 \end{Bmatrix} \tag{3}$$

From the above assumptions, the stiffness matrix of the eth element is given in its local system as follows

$$\mathbf{k}_e = \begin{bmatrix} \frac{EA}{L} & 0 & 0 & -\frac{EA}{L} & 0 & 0 \\ 0 & \frac{12EI_y}{L^3} & \frac{6EI_y}{L^2} & 0 & -\frac{12EI_y}{L^3} & \frac{6EI_y}{L^2} \\ & & \frac{4EI_y}{L} & 0 & -\frac{6EI_y}{L^2} & \frac{2EI_y}{L} \\ & & & \frac{EA}{L} & 0 & 0 \\ & & & & \frac{12EI_y}{L^3} & -\frac{6EI_y}{L^2} \\ \text{sym} & & & & -\frac{6EI_y}{L^2} & \frac{4EI_y}{L} \end{bmatrix} \tag{4}$$

where E, A, L and I_y are the Young's modulus, the cross-sectional area, the length and the inertia moment about the strong $(y-y)$ axis, respectively.

Note that the above formula can be analogously extended for the element weak $(x-x)$ axis by replacing I_y with I_z.

Furthermore, the mass matrix of the eth element is assumed to be lumped at its two ends, its formula in the local system is given by

$$\mathbf{m}_e = \frac{\rho AL}{2} \begin{bmatrix} 1 & 0 & 0 & 0 & 0 & 0 \\ & 1 & 0 & 0 & 0 & 0 \\ & & \varepsilon & 0 & 0 & 0 \\ & & & 1 & 0 & 0 \\ & & & & 1 & 0 \\ \text{sym} & & & & & \varepsilon \end{bmatrix} \tag{5}$$

in which ρ is the material density, and $\varepsilon = 10^{-9}$ denotes a very small value further defined to avoid the singularity when solving the eigenvalue problem in finite element analysis.

Finally, the stiffness and mass matrices of all elements derived in the local system are assembled into the global system using the transform matrix [18].

2.2. *Full model for vibration analysis with damping*

According to the FEM, the vibration analysis with damping of a structure using the full model (FM) can be expressed by the following equation.

$$\mathbf{m}\ddot{\mathbf{u}}(t) + \mathbf{c}\dot{\mathbf{u}}(t) + \mathbf{k}\mathbf{u}(t) = \mathbf{0} \tag{6}$$

where t is the time; $\ddot{\mathbf{u}}$, $\dot{\mathbf{u}}$ and $\mathbf{u}$ denote the acceleration, velocity and displacement vectors, respectively; $\mathbf{m}$, $\mathbf{c}$ and $\mathbf{k}$ are the mass, damping and stiffness matrices, respectively. All the above terms are given in the global system.

Assume that the displacement field is followed by an exponential function in time with the following formula:

$$\mathbf{u}(t) = \mathbf{\Phi} e^{\lambda t} \tag{7}$$

where λ and $\mathbf{\Phi}$ are the eigenvalue and eigenvector, respectively.

Now, substituting Eq. (7) into Eq. (6), one has

$$\left(\lambda^2\mathbf{m} + \lambda\mathbf{c} + \mathbf{k}\right)\mathbf{\Phi} = \mathbf{0} \tag{8}$$

In order to obtain the eigenvalues and eigenvectors, Eq. (8) needs to be rewritten as follows

$$\mathbf{\Gamma}\hat{\mathbf{\Phi}} = \lambda\hat{\mathbf{\Phi}} \tag{9}$$

in which

$$\mathbf{\Gamma} = \begin{bmatrix} \mathbf{0} & \mathbf{I} \\ -\mathbf{m}^{-1}\mathbf{k} & -\mathbf{m}^{-1}\mathbf{c} \end{bmatrix}; \quad \hat{\mathbf{\Phi}} = \begin{Bmatrix} \mathbf{\Phi} \\ \lambda\mathbf{\Phi} \end{Bmatrix} \tag{10}$$

Note that Eq. (9) gives the eigenvalue matrix $\mathbf{\Theta}$ containing the jth eigenvalue λ_j on its main diagonal line. More specifically, λ_j is computed as

$$\lambda_j = -\xi_j\omega_j^{\mathrm{ud}} \pm i\omega_j^{\mathrm{d}} \tag{11}$$

where the jth undamped angular frequency is calculated by

$$\omega_j^{\mathrm{d}} = \mathrm{image}(\lambda_j) \tag{12}$$

And the jth damping ratio is given by

$$\xi_j = -\frac{\mathrm{real}(\lambda_j)}{|\lambda_j|} \tag{13}$$

Meanwhile, the jth damped angular frequency can be attained from the following relationship.

$$\omega_j^{\mathrm{ud}} = \frac{\omega_j^{\mathrm{d}}}{\sqrt{1-(\xi_j)^2}} \tag{14}$$

It can be found from the above equation that ω_j^{ud} is always larger than ω_j^{d} which is caused by the jth damping ratio $\xi_j \in (0, 1)$.

Ultimately, the jth mode shape $\mathbf{\Phi}_j$ can be attained from $\hat{\mathbf{\Phi}}$ which is provided in Eq. (10).

2.3. Model order reduction for vibration analysis with damping

According to Qu et al. [19], for the damped vibration analysis utilizing the MOR in state space, Eq. (6) is rewritten as follows

$$\begin{bmatrix} \mathbf{0} & \mathbf{k} \\ \mathbf{k} & \mathbf{c} \end{bmatrix}\begin{Bmatrix} \mathbf{u} \\ \dot{\mathbf{u}} \end{Bmatrix} + \begin{bmatrix} -\mathbf{k} & \mathbf{0} \\ \mathbf{0} & \mathbf{m} \end{bmatrix}\begin{Bmatrix} \dot{\mathbf{u}} \\ \ddot{\mathbf{u}} \end{Bmatrix} = \begin{Bmatrix} \mathbf{0} \\ \mathbf{0} \end{Bmatrix} \tag{15}$$

Analogously, if $\mathbf{u}(t) = \mathbf{\Phi}e^{\lambda t}$ Eq. (17) can be more shortly rewritten as follows

$$\mathbf{X}\hat{\mathbf{\Phi}} = \mathbf{Y}\hat{\mathbf{\Phi}}\hat{\mathbf{\Sigma}} \tag{16}$$

in which

$$\begin{aligned} \mathbf{X} &= \begin{bmatrix} \mathbf{0} & \mathbf{k} \\ \mathbf{k} & \mathbf{c} \end{bmatrix}; & \mathbf{Y} &= \begin{bmatrix} -\mathbf{k} & \mathbf{0} \\ \mathbf{0} & \mathbf{m} \end{bmatrix} \\ \hat{\mathbf{\Phi}} &= \begin{bmatrix} \mathbf{\Phi} & \mathbf{\Phi}^* \\ \mathbf{\Phi}\mathbf{\Sigma} & \mathbf{\Phi}^*\mathbf{\Sigma}^* \end{bmatrix}; & \hat{\mathbf{\Sigma}} &= \begin{bmatrix} \mathbf{\Sigma} & \mathbf{0} \\ \mathbf{0} & \mathbf{\Sigma}^* \end{bmatrix} \end{aligned} \tag{17}$$

where '*' stands for the complex conjugation.

Due to the orthogonality property, one has

$$\left(\hat{\mathbf{\Phi}}\right)^{\mathrm{T}}\mathbf{X}\hat{\mathbf{\Phi}} = \hat{\mathbf{\Sigma}}; \quad \left(\hat{\mathbf{\Phi}}\right)^{\mathrm{T}}\mathbf{Y}\hat{\mathbf{\Phi}} = \mathbf{I} \tag{18}$$

It is obvious that Eq. (16) fully includes all structural DOFs involving both the so-called master and slave DOFs, which are symbolized as "m" and "s", respectively. For the purpose of removing the slave DOFs "s", Eq. (16) is rewritten as follows

$$\begin{bmatrix}\mathbf{X}_{mm} & \mathbf{X}_{ms}\\ \mathbf{X}_{sm} & \mathbf{X}_{ss}\end{bmatrix}\begin{Bmatrix}\hat{\mathbf{\Phi}}_{mm}\\ \hat{\mathbf{\Phi}}_{sm}\end{Bmatrix} = \begin{bmatrix}\mathbf{Y}_{mm} & \mathbf{Y}_{ms}\\ \mathbf{Y}_{sm} & \mathbf{Y}_{ss}\end{bmatrix}\begin{Bmatrix}\hat{\mathbf{\Phi}}_{mm}\\ \hat{\mathbf{\Phi}}_{sm}\end{Bmatrix}\begin{bmatrix}\mathbf{\Sigma}_{mm} & \mathbf{0}\\ \mathbf{0} & \mathbf{\Sigma}^{*}_{mm}\end{bmatrix} \tag{19}$$

where

$$\mathbf{X}_{mm} = \begin{bmatrix}\mathbf{0} & \mathbf{k}_{mm}\\ \mathbf{k}_{mm} & \mathbf{c}_{mm}\end{bmatrix}; \quad \mathbf{X}_{ms} = (\mathbf{X}_{sm})^{\mathrm{T}} = \begin{bmatrix}\mathbf{0} & \mathbf{k}_{ms}\\ \mathbf{k}_{ms} & \mathbf{c}_{ms}\end{bmatrix}; \quad \mathbf{X}_{ss} = \begin{bmatrix}\mathbf{0} & \mathbf{k}_{ss}\\ \mathbf{k}_{ss} & \mathbf{c}_{ss}\end{bmatrix} \tag{20}$$

$$\mathbf{Y}_{mm} = \begin{bmatrix}-\mathbf{k}_{mm} & \mathbf{0}\\ \mathbf{0} & \mathbf{m}_{mm}\end{bmatrix}; \quad \mathbf{Y}_{ms} = (\mathbf{Y}_{sm})^{\mathrm{T}} = \begin{bmatrix}-\mathbf{k}_{ms} & \mathbf{0}\\ \mathbf{0} & \mathbf{m}_{ms}\end{bmatrix}; \quad \mathbf{Y}_{ss} = \begin{bmatrix}-\mathbf{k}_{ss} & \mathbf{0}\\ \mathbf{0} & \mathbf{m}_{ss}\end{bmatrix} \tag{21}$$

$$\hat{\mathbf{\Phi}}_{mm} = \begin{bmatrix}\mathbf{\Phi}_{mm} & \mathbf{\Phi}^{*}_{mm}\\ \mathbf{\Phi}_{mm}\mathbf{\Sigma}_{mm} & \mathbf{\Phi}^{*}_{mm}\mathbf{\Sigma}^{*}_{mm}\end{bmatrix}; \quad \hat{\mathbf{\Phi}}_{sm} = \begin{bmatrix}\mathbf{\Phi}_{sm} & \mathbf{\Phi}^{*}_{sm}\\ \mathbf{\Phi}_{sm}\mathbf{\Sigma}_{mm} & \mathbf{\Phi}^{*}_{sm}\mathbf{\Sigma}^{*}_{mm}\end{bmatrix}; \quad \hat{\mathbf{\Sigma}}_{mm} = \begin{bmatrix}\mathbf{\Sigma}_{mm} & \mathbf{0}\\ \mathbf{0} & \mathbf{\Sigma}^{*}_{mm}\end{bmatrix} \tag{22}$$

Now, $\hat{\mathbf{\Phi}}_{sm}$ given in Eq. (19) can be eliminated by the following relation.

$$\hat{\mathbf{\Phi}}_{sm} = \mathbf{V}\hat{\mathbf{\Phi}}_{mm} \tag{23}$$

where $\mathbf{V}$ stands for the transform matrix, and it is repeatedly computed as follows

$$\mathbf{V}^{it+1} = \mathbf{X}^{-1}_{mm}\left[(\mathbf{Y}_{sm} + \mathbf{Y}_{ss})\mathbf{V}^{it}\tilde{\mathbf{Y}}^{-1}\tilde{\mathbf{X}} - \mathbf{X}_{ms}\right] \tag{24}$$

where

$$\begin{aligned}\tilde{\mathbf{X}} &= \mathbf{X}_{mm} + \mathbf{X}_{ms}\mathbf{V} + \mathbf{V}^{\mathrm{T}}\mathbf{X}_{sm} + \mathbf{V}^{\mathrm{T}}\mathbf{X}_{ss}\mathbf{V}\\ \tilde{\mathbf{Y}} &= \mathbf{Y}_{mm} + \mathbf{Y}_{ms}\mathbf{V} + \mathbf{V}^{\mathrm{T}}\mathbf{Y}_{sm} + \mathbf{V}^{\mathrm{T}}\mathbf{Y}_{ss}\mathbf{V}\end{aligned} \tag{25}$$

The above iterative process ends when either $\dfrac{\|\mathbf{V}^{it+1} - \mathbf{V}^{it+1}\|_{\text{Frobenius}}}{\|\mathbf{V}^{it+1}\|_{\text{Frobenius}}} \leq 10^{-6}$ or $it = 100$.

Finally, $\hat{\mathbf{\Phi}}_{mm}$ and $\hat{\mathbf{\Sigma}}_{mm}$ can be gained from the following equation.

$$\tilde{\mathbf{X}}\hat{\mathbf{\Phi}}_{mm} = \tilde{\mathbf{Y}}\hat{\mathbf{\Phi}}_{mm}\hat{\mathbf{\Sigma}}_{mm} \tag{26}$$

3. Optimization of sensor locations

3.1. Problem definition

In this section, the problem of optimizing sensor locations of frame structures under damping is presented. Based on the damped vibration responses obtained from the full model (FM) and ROM provided in Sections 2.2. and 2.3, respectively, the optimal sensor placements can be found by maximizing the highest correlation of the **MAC** matrix [20]. More specifically, its coefficients $c^{\text{MAC}}_{i,j}$ are computed as follows

$$c^{\text{MAC}}_{i,j} = \frac{\left(\mathbf{\Phi}^{\mathrm{T}}_{\text{FM},i}\mathbf{\Phi}_{\text{ROM},j}\right)^2}{\left(\mathbf{\Phi}^{\mathrm{T}}_{\text{FM},i}\mathbf{\Phi}_{\text{FM},i}\right)\left(\mathbf{\Phi}^{\mathrm{T}}_{\text{ROM},j}\mathbf{\Phi}_{\text{ROM},j}\right)} \tag{27}$$

in which $\mathbf{\Phi}_{\mathrm{FM},i}$ and $\mathbf{\Phi}_{\mathrm{ROM},j}$ symbolize the ith and jth eigenvectors with damping obtained by the FM and the ROM for all DOFs instead of only "m" DOFs with sensors, respectively. In which, the information on slave DOFs can be fully computed from Eq. (23). In this case, the dimensions of two eigenvectors obtained from both FM and ROM are of the same size.

Then, the above problem can be stated as follows

$$\underset{\mathbf{x}}{\operatorname{argmax}} = \sum\nolimits_{i=1}^{nom} c_{i,i}^{\mathrm{MAC}}(\mathbf{x}) \tag{28}$$

where $\mathbf{x} = \{x_1, \ldots, x_{nos}\}$ denotes the discrete design variable vector containing nos number of sensor locations.

3.2. Particle swarm optimization

The PSO is known as a population-based metaheuristic optimization algorithm originally proposed by Kennedy and Eberhart [21]. Then, it is refined by Shi and Eberhart [22]. This algorithm is inspired by the collective foraging behavior of bird flocks and fish schools. This PSO has been applied to a large number of publications in numerous fields. More thorough surveys of this algorithm can be found in Refs. [23, 24]. In the PSO, each candidate solution is modeled as a particle whose positions are updated via the exploration ability in a given search space by the swarm evolution with the collective knowledge. More concretely, the procedure of the PSO is detailed below.

a. Initialization

Before the optimization process, the position of the jth design variable of the ith particle is initialized as follows

$$x_{i,j} = x_j^{\min} + rand_{i,j}[0,1]\left(x_j^{\max} - x_j^{\min}\right); \quad i = 1 \rightarrow n_p; \quad j = 1 \rightarrow n_d \tag{29}$$

where $x_j^{\min}$ and $x_j^{\max}$ stand for the minimum and maximum boundaries of the jth design variable, respectively; $rand_{i,j}[0,1]$ denotes a number randomly given in $[0,1]$. n_p and n_d symbolize the swarm size and the number of design variables, respectively.

b. Velocity update

In the PSO, the location of the ith particle at the kth iteration is updated via its velocity. More concretely, the particle motion is represented as follows

$$\mathbf{v}_i^{k+1} = \chi \mathbf{v}_i^k + c_1 r_1 \left(\mathbf{p}_i - \mathbf{x}_i^k\right) + c_2 r_2 \left(\mathbf{g} - \mathbf{x}_i^k\right), \tag{30}$$

where the inertia weight $\chi = \chi_{\max} - \dfrac{\chi_{\max} - \chi_{\min}}{k_{\max}} k$ ($\chi_{\max} = 0.9, \chi_{\min} = 0.4$) is used to control the balance between the global exploration ability and local exploitation capbility; $c_1 = 2$ and $c_2 = 2$ denote the cognitive and social acceleration coefficients, respectively; $r_1, r_2 \in [0,1]$ stand for two random scalar values; $\mathbf{p}_i$ is the best ith position found by the particle itself up to the current iteration, and $\mathbf{g}$ denotes the global best location searched by any particles in the entire swarm up to the current iteration.

c. Position update

Next, the position of the ith particle at the current iteration is updated by the following equation.

$$\mathbf{x}_i^{k+1} = \mathbf{x}_i^k + \mathbf{v}_i^{k+1} \tag{31}$$

It is clear that, in this step, if the location of the ith particle exceeds its minimum and maximum boundaries, it is penalized to return to the initial design space.

d. Fitness evaluation and selection

In this stage, by evaluating all the fitness values obtained by the particle locations newly updated from Eq. (31), $\mathbf{p}_i$ and $\mathbf{g}$ are then extracted for the next iteration.

3.3. Several modifications for particle swarm optimization

In the original PSO, design variables are continuously initialized by Eq. (29). However, in the present optimization problem as defined in Eq. (28), sensor locations corresponding to the labels of structural DOFs are treated as discrete design variables. In this case, that formula can not be applied, and thus it needs to be modified to meet the current requirement.

Now, the position of the jth design variable of the ith particle in the first step is modified as follows

$$x_{i,j} = randi_{i,j}[1, nos]; \quad i = 1 \rightarrow n_p; \quad j = 1 \rightarrow n_d \tag{32}$$

where $randi_{i,j}[1, nos]$ yields a random integer number in $[1, nos]$.

Moreover, if the location newly updated by Eq. (31) violates the given design domain, it is dealt with as follows

$$x_{i,j}^{k+1} = \begin{cases} 2x_j^{\min} - x_{i,j}^{k+1}, & x_{i,j}^{k+1} < 1 \\ 2x_j^{\max} - x_{i,j}^{k+1}, & x_{i,j}^{k+1} > nos \\ x_{i,j}^{k+1}, & \text{otherwise} \end{cases} \tag{33}$$

Note that Eq. (33) results in continuous variables, hence, their nearest integer is rounded [25].

In this work, the swarm size n_p is chosen as 20. The maximum iteration number $k_{\max}$ is 100. And each case is run 5 times. Then, the only outcomes obtained by the best run are reported.

4. Results and discussion

4.1. 2D one-storey frame

As a first demonstration studied in this work, a 2D one-storey frame with 15 elements as shown in Fig. 1 is presented. Nodes 1 and 16 are fixed. All the beams and columns are designed with the same material features, with the material density of 7860 kg/m^3 and Young's modulus of 210 GPa. Furthermore, the same section of 0.00635 m × 0.0760 m is assigned to them. This frame modeling is referred to Seyedpoor et al. [26]. In this work, the damping influence is further taken into account based on the Rayleigh damping [27]. More specifically, the damping matrix $\mathbf{c}$ in the global system is computed by

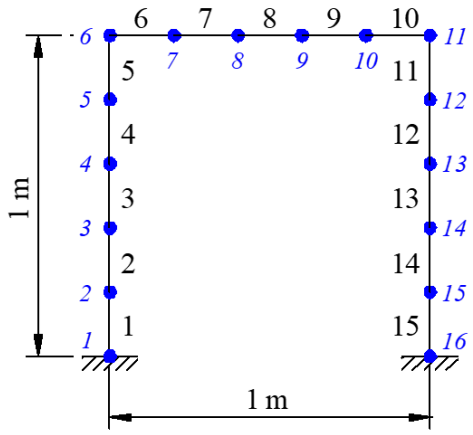


Figure 1. A 2D one-storey frame with 15 elements

$$\mathbf{c} = \eta_1 \mathbf{m} + \eta_2 \mathbf{k} \tag{34}$$

with

$$\eta_1 = \xi \frac{2\omega_1^{\text{ud}}\omega_2^{\text{ud}}}{\omega_1^{\text{ud}} + \omega_2^{\text{ud}}}; \quad \eta_2 = \xi \frac{2}{\omega_1^{\text{ud}} + \omega_2^{\text{ud}}} \tag{35}$$

in which the damping ratio ξ is assumed to be 5% for all investigated cases, unless otherwise specified; ω_1^{ud} and ω_2^{ud} denote the first two undamped angular frequencies.

Firstly, 5 sensors are utilized. As before indicated in the Introduction section, measuring the signals at rotational DOFs is quite difficult due to the executable conditions. Hence, all rotational DOFs are excluded in the given design space. As a consequence, the only two vertical and horizontal DOFs are considered as potential ones for installing sensors. Table 1 reports the optimal sensor locations attained by the PSO. Fig. 2 displays the **MAC** matrix attained by the above sensor placements. It can be found that this matrix has a high correlation, where most of the coefficients on the main diagonal line are 1, while the others are zero. The convergence process for the 2D one-storey frame with 5 optimal sensor locations Fig. 3. Next, the Rayleigh damping ratio of 3% is further investigated. As reported in Table 2, 5 optimal sensor locations in this case are totally different from those given in Table 1 with $\xi = 5\%$. It is clear that optimal sensor locations are relatively sensitive to different damping intensities. The **MAC** matrix and the convergence history obtained with $\xi = 3\%$ are displayed in Fig. 4 and Fig. 5, respectively. It is seen that the value of the objective function is better when the damping amplitude is smaller.

Table 1. 5 sensor locations optimized for the 2D one-storey frame with $\xi = 5\%$

Node	Horizontal DOF	Vertical DOF	Rotational DOF
5		✓	
7		✓	
10	✓	✓	
12		✓	

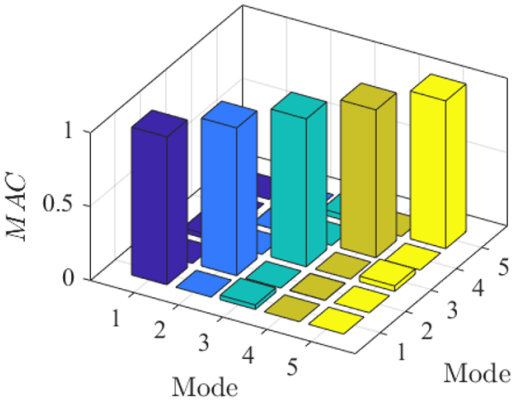


Figure 2. The MAC matrix acquired by 5 optimal sensor locations for the 2D one-storey frame with $\xi = 5\%$

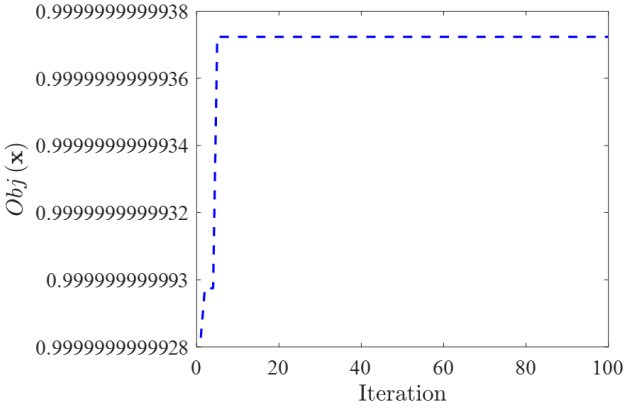


Figure 3. The convergence process acquired by 5 optimal sensor locations for the 2D one-storey frame with $\xi = 5\%$

Table 2. 5 sensor locations optimized for the 2D one-storey frame with $\xi = 3\%$

Node	Horizontal DOF	Vertical DOF	Rotational DOF
2	✓		
7	✓		
13	✓		
10		✓	
11		✓	

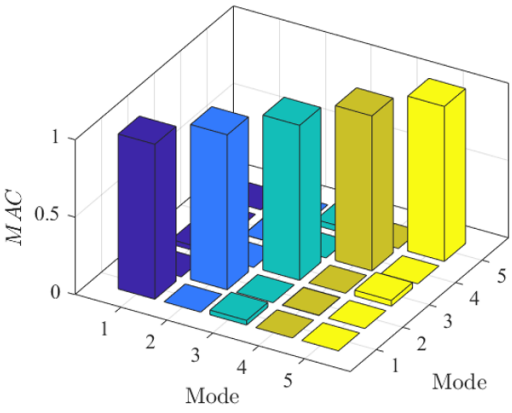


Figure 4. The MAC matrix acquired by 5 optimal sensor locations for the 2D one-storey frame with $\xi = 3\%$

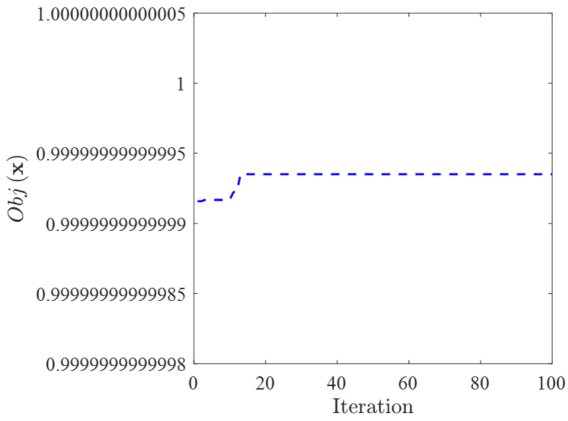


Figure 5. The convergence process acquired by 5 optimal sensor locations for the 2D one-storey frame with $\xi = 3\%$

Now, the result of 8 sensor locations optimized by the PSO is reported in Table 3. Analogously, rotational DOFs are also curtailed in the design domain instead of installing all DOFs. The **MAC** matrix and its convergence history for this case are plotted in Fig. 6 and Fig. 7, respectively.

Table 3. 8 sensor locations optimized for the 2D one-storey frame for the 2D one-storey frame

Node	Horizontal DOF	Vertical DOF	Rotational DOF
2	✓		
5	✓		
8	✓		
11	✓		
14	✓		
6		✓	
7		✓	
15		✓	

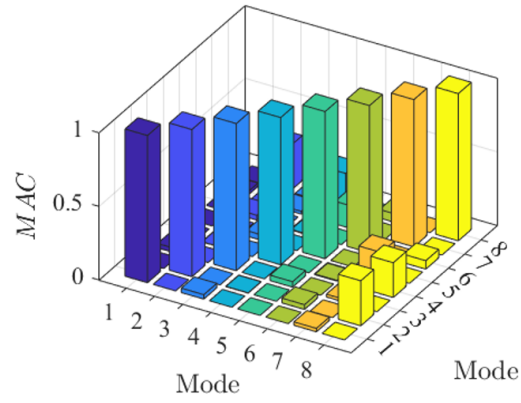


Figure 6. The MAC matrix acquired by 8 optimal sensor locations for the 2D one-storey frame

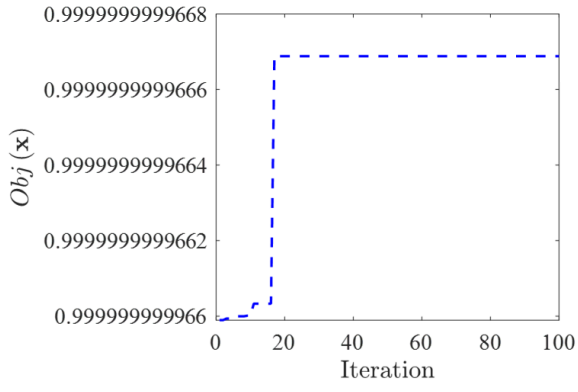


Figure 7. The convergence process acquired by 8 optimal sensor locations for the 2D one-storey frame

For evaluating the damping effect on the angular frequencies with and without damping, the results obtained by the ROM are summarized in Table 4 and Table 5. It is clear that the angular fre-

quencies with damping are always smaller than those without damping. This can be easily recognized by the formula given in Eq. (14). The damping influence on higher-order angular frequencies is more significant than lower-order ones. In addition, in order to verify the reliability and accuracy of the proposed method, a comparison of the undamped angular frequencies attained by this study with the full model in Sap2000 is also reported in the above tables. Note that in that software, the Timoshenko theory is utilized to simulate beams and columns. Therefore, for the consistency of comparative outcomes of two different beam theories, the shear deformation effect on beam and column sections in Sap2000 is ignored by assigning the Poisson's ratio to zero. Moreover, the shear areas of beams and columns are assigned to 10^9 to yield an extremely small shear deformation effect on section. As known, Sap2000 cannot resolve the eigenvalue problem with damping as defined in Eq. (8). As a result, the only undamped angular frequencies are reported and compared. It can be found from the above tables that a high compatibility of undamped angular frequencies is observed. This confirms the high accuracy and reliability of the proposed methodology presented in this study.

Table 4. The first five angular frequencies obtained by 5 sensor locations with and without damping

Mode	This study		Sap2000
	ω_j^{d} (rad/s)	ω_j^{ud} (rad/s)	ω_j^{d} (rad/s)
1	361.6443	362.0972	362.0972
2	1417.8761	1419.6518	1419.6518
3	2311.5435	2317.4345	2317.4346
4	2472.4441	2479.5020	2479.5020
5	4778.1250	4824.5394	4824.5395

Table 5. The first ten angular frequencies obtained by 8 sensor locations with and without damping for the 2D one-storey frame

Mode	This study		Sap2000
	ω_j^{d} (rad/s)	ω_j^{ud} (rad/s)	ω_j^{d} (rad/s)
1	361.6443	362.0972	362.0972
2	1417.8761	1419.6518	1419.6518
3	2311.5435	2317.4345	2317.4346
4	2472.4441	2479.5020	2479.5020
5	4778.1250	4824.5394	4824.5395
6	5972.5894	6063.5223	6063.5225
7	6415.5523	6528.7676	6528.7677
8	7003.6615	7152.1688	7152.1689

4.2. 2D four-storey frame

Herein, a 2D four-storey frame with 45 elements as plotted in Fig. 8 is examined. All the column bases are assumed to be fully fixed. The material utilized in this frame has a density of 7780 kg/m^3 and Young's modulus of 210 GPa. Moreover, the columns have the same section of W14x145, whilst the beams have the same section of W12x87. This frame was modeled by Seyedpoor et al. [26] without considering damping. Similar to the previous example, the damping effect is considered by the Rayleigh damping [27] with the damping ratio $\xi = 5\%$ as a typical illustration.

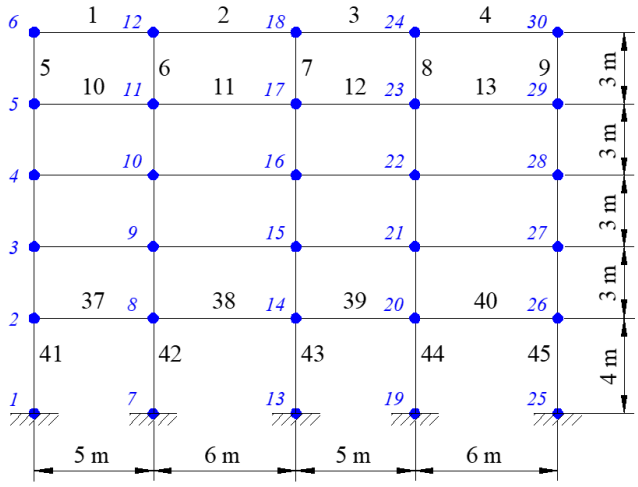


Figure 8. A 2D four-storey frame with 45 elements

10 and 15 sensor locations optimized for the 2D four-storey frame are shown in Table 6, Table 7 and Table 8, respectively. The **MAC** matrix and the convergence process with those optimal sensor locations are plotted in Fig. 9 and Fig. 10 for 10 sensors, Fig. 11 and Fig. 12 for 15 sensors, Fig. 13 and Fig. 14 for 20 sensors, respectively. Additionally, the angular frequencies obtained by the ROM in this study with and without damping for both cases are reported in Table 9, Table 10 and Table 11. As expected, the undamped angular frequencies given by Sap2000 are in good agreement with those of the present method. In the case of 20 sensors, the eigenvectors of modes 16 and 20 obtained by the FM and the ROM are not consistent with each other, as seen in Fig. 13, these two modes can be remarkably dominated by rotational DOFs which are ignored in the solution domain of the optimization problem. Nonetheless, for such high-order modes, their contribution is negligible for most engineering problems in practice. And thus, they can be neglected without loss of accuracy in the dynamic analysis. Indeed, as reported in Table 12, the modal participating mass ratio of the first three modes exceeds 99%, and this ratio almost reaches 100% for the first ten modes. This reveals that low modes are more dominant than higher-order ones. These outcomes have indicated the ability of the current approach to optimize the sensor positions of frames considering damping with many applications to the SHM.

Table 6. 10 sensor locations optimized for the 2D four-storey frame

Node	Horizontal DOF	Vertical DOF	Rotational DOF
8	✓		
15	✓		
16	✓		
17	✓		
18	✓		
4		✓	
9		✓	
16		✓	
22		✓	
28		✓	

Table 7. 15 sensor locations optimized for the 2D four-storey frame

Node	Horizontal DOF	Vertical DOF	Rotational DOF
3	✓		
4	✓		
6	✓		
9	✓		
10	✓		
12	✓		
14	✓		
17	✓		
20	✓		
23	✓		
2		✓	
10		✓	
16		✓	
23		✓	
27		✓	

Table 8. 20 sensor locations optimized for the 2D four-storey frame

Node	Horizontal DOF	Vertical DOF	Rotational DOF
5	✓	✓	
6	✓		
10	✓		
11	✓		
12	✓		
14	✓		
15	✓		
16	✓	✓	
20	✓		
21	✓		
22	✓		
23	✓		
26	✓		
27	✓		
3		✓	
24		✓	
28		✓	
29		✓	

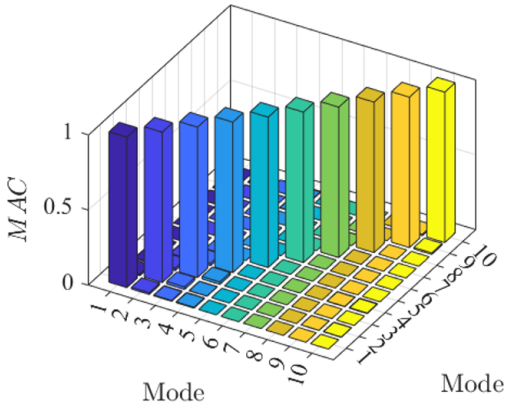


Figure 9. The MAC matrix acquired by 10 optimal sensor locations for the 2D four-storey frame

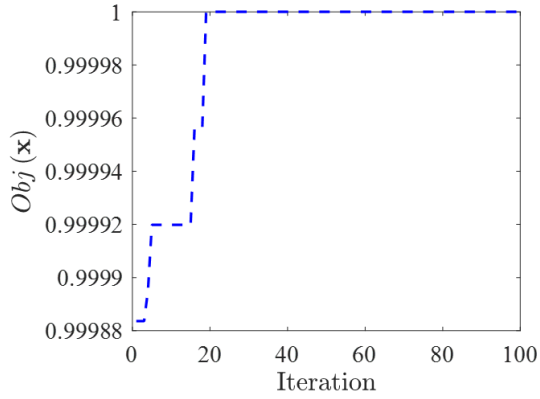


Figure 10. The convergence process for the 2D four-storey frame with 10 optimal sensor locations

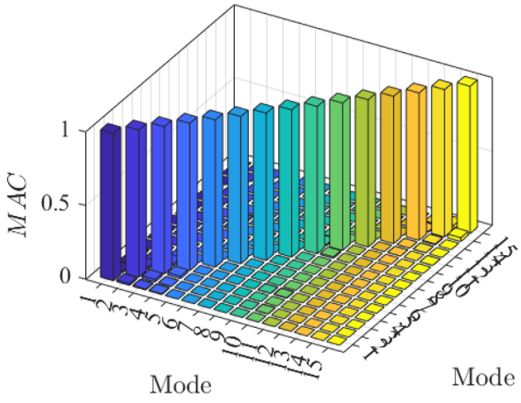


Figure 11. The MAC matrix acquired by 15 optimal sensor locations for the 2D four-storey frame

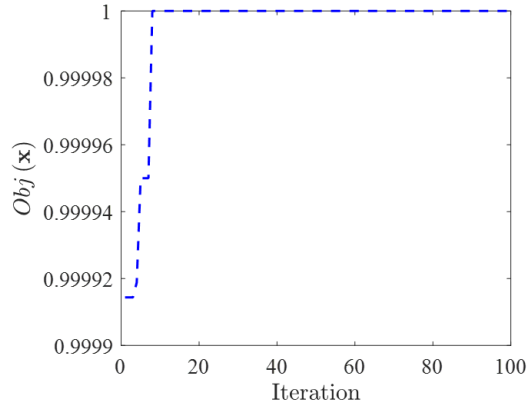


Figure 12. The convergence process for the 2D four-storey frame with 15 optimal sensor locations

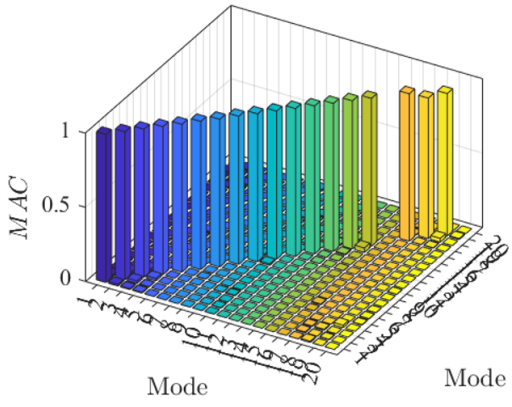


Figure 13. The MAC matrix acquired by 20 optimal sensor locations for the 2D four-storey frame

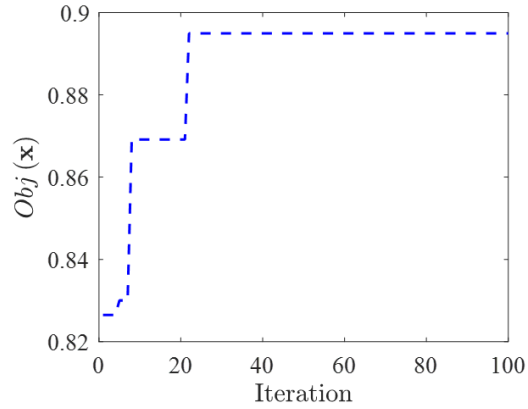


Figure 14. The convergence process for the 2D four-storey frame with 20 optimal sensor locations

Table 9. The first ten angular frequencies obtained by 10 sensor locations with and without damping for the 2D four-storey frame

Mode	This study		Sap2000
	ω_j^{d} (rad/s)	ω_j^{ud} (rad/s)	ω_j^{d} (rad/s)
1	29.1673	29.2038	29.2038
2	95.4094	95.5289	95.5289
3	182.0486	182.6242	182.6242
4	292.0764	294.2658	294.2658
5	333.4358	336.6701	336.6701
6	340.4338	343.8740	343.8740
7	349.1563	352.8658	352.8658
8	387.4958	392.5667	392.5667
9	403.6495	409.3873	409.3873
10	406.5615	412.4258	412.4258

Table 10. The first fifteen angular frequencies obtained by 15 sensor locations with and without damping for the 2D four-storey frame

Mode	This study		Sap2000
	ω_j^{d} (rad/s)	ω_j^{ud} (rad/s)	ω_j^{d} (rad/s)
1	29.1673	29.2038	29.2038
2	95.4094	95.5289	95.5289
3	182.0486	182.6242	182.6242
4	292.0764	294.2658	294.2658
5	333.4358	336.6701	336.6701
6	340.4338	343.8740	343.8740
7	349.1563	352.8658	352.8658
8	387.4958	392.5667	392.5667
9	403.6495	409.3873	409.3873
10	406.5615	412.4258	412.4258
11	459.2293	467.7394	467.7394
12	475.3005	484.7640	484.7640
13	517.9016	530.2637	530.2637
14	566.1270	582.4987	582.4987
15	615.7394	637.1697	637.1697

Table 11. The first fifteen angular frequencies obtained by 20 sensor locations with and without damping for the 2D four-storey frame

Mode	This study		Sap2000
	ω_j^{d} (rad/s)	ω_j^{ud} (rad/s)	ω_j^{ud} (rad/s)
1	29.4740	29.4952	29.2038
2	95.4194	95.5389	95.5289
3	182.0494	182.6249	182.6242
4	292.0883	294.2792	294.2658
5	333.5447	336.8112	336.6701
6	340.9270	344.5914	343.8740
7	349.2602	353.0324	352.8658
8	387.4961	392.5671	392.5667
9	403.8370	409.5918	409.3873
10	406.6534	412.5571	412.4258
11	459.2248	467.7365	467.7394
12	475.1822	484.5965	484.7640
13	517.6167	529.8304	530.2637
14	566.2813	582.9957	582.4987
15	613.5662	634.2942	637.1697
16	802.4500	852.6973	848.3603
17	819.8177	873.9103	871.0546
18	851.3259	913.9792	899.1698
19	1059.6377	1173.7691	954.3532
20	-	-	977.0785

Table 12. Modal participating mass ratio of the 2D four-storey frame with 20 optimal sensor locations

Mode	Effective mass	Modal participating mass ratio (%)
1	25107.4442	86.23
2	2886.3596	96.14
3	**837.4085**	**99.02**
4	239.4917	99.84
5	0.0389	99.84
6	0.1090	99.84
7	1.2838	99.85
8	0.2129	99.85
9	16.7758	99.91
10	**27.3874**	**100**
11	0.0010	100
12	0.0022	100
13	0.0070	100
14	0.0101	100
15	0.0006	100
16	0.0408	100

Mode	Effective mass	Modal participating mass ratio (%)
17	0.0069	100
18	0.0739	100
19	0.0008	100

5. Conclusions

An effective strategy for finding out the best sensor placements of frame structures with the damping influence has been presented in this work. In which, by maximizing the highest correlation in the **MAC** matrix calculated by the eigenvectors between the FM and the ROM for the first ten shape modes, the best positions for locating measurement sensors at DOFs can be searched by the PSO. Several modifications to the original PSO are suggested to deal with discrete variables assigned to the labels at DOFs instead of the continuous ones as in its original. The current approach allows to exclude rotational DOFs as well as practically unmeasured DOFs owing to complex conditions by giving a design space for sensor locations. Two frame structures involving a 2D one-storey frame and a 2D four-storey frame are selected to illustrate the ability of the present method. Applications of the attained outcomes are fully potential for the SHM.

Acknowledgment

This research is funded by Vietnam National Foundation for Science and Technology Development (NAFOSTED) under grant number 107.02-2025.13.

Declaration of generative AI and AI-assisted technologies

The author(s) declare that no generative AI or AI-assisted technologies were used in the preparation of this manuscript.

References

[1] Gharehbaghi, V. R., Noroozinejad Farsangi, E., Noori, M., Yang, T. Y., Li, S., Nguyen, A., Málaga-Chuquitaype, C., Gardoni, P., Mirjalili, S. (2022). A critical review on structural health monitoring: Definitions, methods, and perspectives. *Archives of Computational Methods in Engineering*, 29(4):2209–2235.

[2] Katam, R., Pasupuleti, V. D. K., Kalapatapu, P. (2023). A review on structural health monitoring: Past to present. *Innovative Infrastructure Solutions*, 8(9):248.

[3] Zhang, B., Ren, Y., He, S., Gao, Z., Li, B., Song, J. (2025). A review of methods and applications in structural health monitoring (SHM) for bridges. *Measurement*, 245:116575.

[4] Sun, Z., Mahmoodian, M., Sidiq, A., Jayasinghe, S., Shahrivar, F., Setunge, S. (2025). Optimal sensor placement for structural health monitoring: A comprehensive review. *Journal of Sensor and Actuator Networks*, 14(2):22.

[5] Kim, T., Youn, B. D., Oh, H. (2018). Development of a stochastic effective independence (SEFI) method for optimal sensor placement under uncertainty. *Mechanical Systems and Signal Processing*, 111:615–627.

[6] He, C., Xing, J., Li, J., Yang, Q., Wang, R., Zhang, X. (2015). A new optimal sensor placement strategy based on modified modal assurance criterion and improved adaptive genetic algorithm for structural health monitoring. *Mathematical Problems in Engineering*, 2015(1):626342.

[7] Kim, S.-H., Cho, C. (2024). Effective independence in optimal sensor placement associated with general Fisher information involving full error covariance matrix. *Mechanical Systems and Signal Processing*, 212:111263.

[8] Nasr, D. E., Saad, G. A. (2017). Optimal sensor placement using a combined genetic algorithm–ensemble Kalman filter framework. *ASCE-ASME Journal of Risk and Uncertainty in Engineering Systems, Part A: Civil Engineering*, 3(1):04016010.

[9] Yi, T.-H., Li, H.-N., Zhang, X.-D. (2012). A modified monkey algorithm for optimal sensor placement in structural health monitoring. *Smart Materials and Structures*, 21(10):105033.
[10] Tong, K. H., Bakhary, N., Kueh, A. B. H., Yassin, A. Y. M. (2014). Optimal sensor placement for mode shapes using improved simulated annealing. *Smart Structures and Systems*, 13(3):389–406.
[11] Yi, T.-H., Zhou, G.-D., Li, H.-N., Wang, C.-W. (2017). Optimal placement of triaxial sensors for modal identification using hierarchic wolf algorithm. *Structural Control and Health Monitoring*, 24(8):e1958.
[12] Dinh-Cong, D., Dang-Trung, H., Nguyen-Thoi, T. (2018). An efficient approach for optimal sensor placement and damage identification in laminated composite structures. *Advances in Engineering Software*, 119:48–59.
[13] Matsushita, K. Y., Miguel, L. F. F., Villalba-Morales, J. D. (2025). Optimal sensor placement for modal identification of large truss structures using the Circle-Inspired optimization algorithm. *Evolutionary Intelligence*, 18(6):117.
[14] Lee, E.-T., Eun, H.-C. (2022). Optimal sensor placement in reduced-order models using modal constraint conditions. *Sensors*, 22(2):589.
[15] Lieu, Q. X. (2024). An optimization-assisted reduced order model for dynamics of plates using isogeometric analysis. *Thin-Walled Structures*, 202:112078.
[16] Lieu, Q. X. (2023). A novel multistage damage detection method for trusses using time-history data based on model order reduction and deep neural network. *Mechanical Systems and Signal Processing*, 200:110635.
[17] Reddy, J. (2005). *An introduction to the finite element method*. 3rd edition, McGraw-Hill Education.
[18] Yang, Y.-B., Kuo, S.-R. (1994). *Theory & analysis of nonlinear framed structures*. Prentice Hall.
[19] Qu, Z.-Q., Selvam, R. P., Jung, Y. (2003). Model condensation for non-classically damped systems—Part II: Iterative schemes for dynamic condensation model. *Mechanical Systems and Signal Processing*, 17 (5):1017–1032.
[20] Pastor, M., Binda, M., Harčarík, T. (2012). Modal assurance criterion. *Procedia Engineering*, 48:543–548.
[21] Kennedy, J., Eberhart, R. (1995). Particle swarm optimization. In *Proceedings of ICNN'95 - International Conference on Neural Networks*, 4:1942–1948.
[22] Shi, Y., Eberhart, R. (1998). A modified particle swarm optimizer. In *1998 IEEE International Conference on Evolutionary Computation Proceedings. IEEE World Congress on Computational Intelligence*, 69–73.
[23] Wang, D., Tan, D., Liu, L. (2018). Particle swarm optimization algorithm: An overview. *Soft Computing*, 22(2):387–408.
[24] Shami, T. M., El-Saleh, A. A., Alswaitti, M., Al-Tashi, Q., Summakieh, M. A., Mirjalili, S. (2022). Particle swarm optimization: A comprehensive survey. *IEEE Access*, 10:10031–10061.
[25] Lieu, Q. X., Do, D. T. T., Lee, J. (2018). An adaptive hybrid evolutionary firefly algorithm for shape and size optimization of truss structures with frequency constraints. *Computers & Structures*, 195:99–112.
[26] Seyedpoor, S. M., Ahmadi, A., Pahnabi, N. (2019). Structural damage detection using time domain responses and an optimization method. *Inverse Problems in Science and Engineering*, 27(5):669–688.
[27] Clough, R. W. (2015). *Dynamics of structures*. 2nd edition, CBS Publishers and Distributors PVT LTD.